applied optics

Electric-field-induced band bending on GaN: *in situ* effects of electron beam irradiation on time-dependent cathodoluminescence

Eva M. Campo,[1,*] Milan Pophristic,[2] Laurel Hopkins,[1] and Ian T. Ferguson[3]

[1]School of Electronic Engineering, Bangor University, Gwynedd LL57 1UT, UK
[2]Department of Chemistry and Biochemistry, University of the Sciences, Philadelphia, Pennsylvania 19104, USA
[3]Department of Electrical and Computer Engineering, University of North Carolina at Charlotte, Charlotte, North Carolina 28223, USA
*Corresponding author: e.campo@bangor.ac.uk

Received 13 January 2015; revised 19 March 2015; accepted 20 March 2015; posted 20 March 2015 (Doc. ID 231586); published 14 April 2015

Electron beam bombardment of GaN has been monitored by secondary electron (SE), cathodoluminescence (CL) imaging, simultaneous *in situ* CL, and specimen current (SC) measurements. Under extreme irradiation conditions, system perturbations, as seen by SE and time-dependent CL, are attributed to internal charge dynamics extending beyond the scanned areas. Under moderate irradiation conditions, the size of affected regions correlates with nominal scanned regions. Time-dependent CL at the near band edge (NBE) revealed complex interplay with SC, which was modeled through band bending at the Au/GaN interface. The system has shown distinctive internal electric field dynamics upon sample handling, affecting both time-dependent CL spectra and SC as well as producing contrast reversal in SE imaging, to which humidity adsorption could be contributing. The band-bending model presented here can account for both moderate irradiation and humidity effects through variations of depletion widths and Schottky barrier heights. Our findings are consistent with current models where e-beam activated V_{Ga} promotes decreased NBE intensities and C_N promotes DL emissions.

OCIS codes: (250.1500) Cathodoluminescence; (160.2540) Fluorescent and luminescent materials; (160.6000) Semiconductor materials.

http://dx.doi.org/10.1364/AO.54.003613

1. INTRODUCTION

Outstanding development of hyperspectral CL builds upon abundant technological improvements in electron microscopy systems achieved in the last few decades, leading to improved vacuum systems and higher-brightness emission guns, and enabling CL acquisition with unprecedented signal to noise levels and resolution [1,2]. The wealth of information embedded in cathodoluminescence (CL) spectra allows for strain assessment, electron-hole recombination efficiency, and overall optical mapping of technologically relevant materials such as gallium nitride (GaN) [3]. Indeed, CL has proven extremely useful to the development of this intricate III–V material system early on [4], allowing identification of the still chemically uncertain and pervasive deep level emission at 560 nm [5]. However, e-beam irradiation has been reported to affect near band edge (NBE) CL in GaN [6], with the possibility of contamination-induced adsorption being ruled out earlier [7].

Indeed, CL dynamics upon e-beam irradiation remain poorly understood, often attributed to charging processes [7] and derived effects such as electromigration of impurities [8,9], e-beam-induced defects [8], and more recently to humidity adsorption [6]. In fact, humidity effects by way of humidity adsorption have been recently shown to radically alter surface conductivity in chemical vapor deposition–grown diamond [10]. Albeit the effects of electron beam irradiation on spectroscopies is still an unresolved and highly relevant issue, with all, charging dynamics reports remain a highly topical theme [11].

Moreover, the relevance of charging dynamics is especially impactful in CL. Understanding this phenomenology is a doorway to infer device operation and subsequent degradation, providing deep insights into unresolved defect dynamics within GaN in particular [12]. Meneghini *et al.* attributed the degraded operation of indium gallium nitride/gallium nitride (InGaN/GaN) laser diodes to increased nonrecombination efficiency upon aging. Furthermore, Nykänen confirmed the activation of Ga vacancy defects (V_{Ga}) upon low-energy electron beam irradiation conditions that emulate device operation [13,14]. The regained interest in CL analysis [1,15], through a variety of fields inclusive of metamaterials [9], is promoting studies on time-resolved and time-dependent CL (t-CL). The

former aims to address emission lifetimes [16] and the latter to unveil a plethora of physical phenomena, often providing insight into device operation and failure [12–14]. The underlying phenomena are the result of complex interplay between carriers and extended defects [8,13,14,17], as well as surface states nucleating upon device operation [1,6,17] in addition to V_{Ga} activation [13,14]. This complexity has been identified as generation of stacking faults [8] and the activation of spontaneous polarization fields owing to surface charge desorption [18].

In this work, we advance the current knowledge in t-CL by simultaneously observing the evolution of specimen current (t-SC) during irradiation, yielding a band-bending model governed by charge dynamics. The purpose of these experiments was to assess dynamics of secondary electron (SE) and CL-degraded areas and to determine the influence of electron beam irradiation on luminescence from the window region in lateral epitaxial overgrown (LEO) GaN [17,19]. Experiments also investigated the effects of unintended humidity adsorption on near band edge CL (NBE-CL) intensity and on SE yield, given the prior-established importance of surface states in GaN [18]. Understanding of electric-field effects on GaN, inclusive of water adsorption effects [20], will offer insights into optoelectronics aging and device performance [12,13], as well as identify opportunities toward radiation-hard electronics and microsystems in harsh environments [21,22].

2. EXPERIMENT

CL measurements were conducted at room temperature in a JEOL JSM-6400 scanning electron microscope (SEM) equipped with a tungsten source and an Oxford Instruments CF302 CL system with parabolic mirror light-collecting optics, computer-controlled SPEX 340S spectrometer, and a Hamamamtsu-R928 gallium arsenide (GaAs) photomultiplier tube (PMT). Output from PMT can be used to acquire CL spectra by measuring CL intensity at different wavelengths (wavelength scans), to measure CL intensity at a particular wavelength through t-CL, or to form monochromatic CL images. A Gatan Digiscan unit acquired SE and CL images digitally. A Keithley 427 current amplifier was connected between the specimen stage and the grounding system to measure SC as a function of time.

A nominally undoped GaN film was grown by metal organic chemical vapor deposition (MOCVD) in an Emcore Spectrablue reactor at Emcore Corp. LEO–GaN on sapphire growth used a 9 μm wide window, 100 nm thick SiNx mask, and a 2 μm thick GaN buffer layer at 1050°C and 50 Torr. GaN was then grown in the window regions with lateral overgrowth over adjacent regions of the mask. Properties of window and laterally grown areas differ greatly in impurity and defect density [9,15,19]. A 50 Å gold–palladium (Au–Pd) coating layer was sputter-coated on the GaN surface to minimize charging effects, and electrical contact was made from the coating layer to the sample holder by conductive carbon tape. In this scheme, with one single contact from the stage to the current amplifier, the specimen current is measured rather than an electron-beam-induced current. Electron beam irradiation was performed through the Au–Pd contacts, and both CL and SC measurements were acquired.

Window regions were irradiated from the top. SEM and CL images were acquired on all the regions previously scanned with 20 keV and 20 nA (400 μW, extreme irradiation conditions) or 10 keV and 1 nA (10 μW, moderate irradiation conditions) under different magnifications for 1000 or 2000 s. Experiments were conducted under a vacuum of 2×10^{-6} Torr. Three stages of vacuum were provided by rotary, turbo, and ion pumps; the latter ensured that oil-derived residue from mechanical pumps was absent from the vacuum system. The vacuum conditions provided repeatable SE, CL, and SC experimental results. Digital imaging was set at 300 × 300 pixels, 54 μs dwell time for SEM imaging, and 10 ms dwell time for CL imaging.

3. SE AND NBE-CL EMISSION DISTRIBUTION UNDER EXTREME IRRADIATION

A. Effects of Magnification

At electron beam settings of 20 keV and 20 nA, CL spectra revealed NBE and intense deep level (DL) emissions at 365 and 570 nm, respectively (Fig. 1), as expected from this highly defective region. Monochromatic time-dependent CL spectra were recorded *in situ* during e-beam irradiation at 15, 30, 60, and 120 kx magnification for 1000 s. Secondary electron emission signals increased from the irradiated regions, as seen in Fig. 2(a), at 30 kx. Conversely, NBE-CL images showed decreased emissions from irradiated regions at all magnifications [Fig. 2(b)].

Intensity line profiles determined the size of affected regions in the SE and CL images. The widths of affected regions as seen in SE (SEW) were measured by line scan profiles, as shown in Fig. 2(c). Two levels of degradation, complete and partial, can be identified in the line scan profile from NBE-CL imaging in Fig. 2(d), which corresponds to the 30 kx irradiation setting. The level at 12,000 a.u. defines a completely degraded region coinciding with background noise from these acquisition conditions.

The partially degraded state can be conveniently assessed in line scan profiles, as seen in Fig. 2(d), where CL intensity is continuously increased from a fully degraded background to

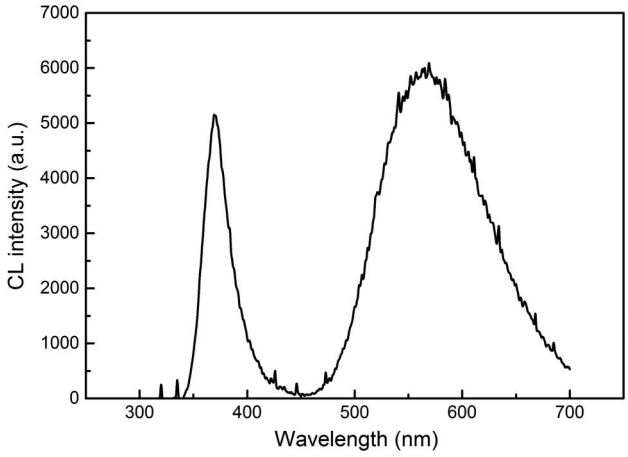

Fig. 1. Wavelength CL scan on window regions at 15 kx magnifications.

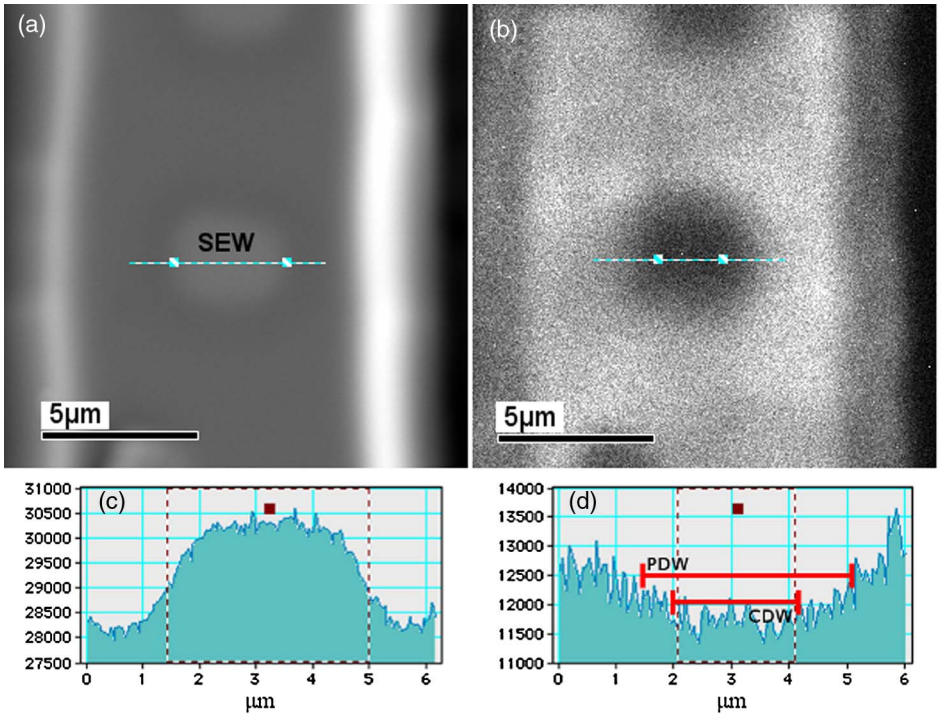

Fig. 2. (a) SE image of irradiated region at 30 kx magnification, SEW highlighted by blue line profile with markers at irradiation boundaries. (b) NBE-CL image of same region as (a), also with line profile. (c) SE line scan profile. (d) NBE-CL line profile intensity highlighting PDW and CDW.

the level of surrounding nonirradiated areas. Sizes of partially degraded regions were determined by measuring the distance that corresponds to 10% decrease from the nonirradiated regions. Line intensity profile in Fig. 2(d) shows completely and partially degraded widths (CDW and PDW, respectively) of 2.0 and 3.5 μm, respectively, at 30 kx. Similar experiments were run at 15, 30, 60, and 120 kx magnifications, and the results are plotted in Fig. 3.

Irradiation at 15 kx magnification for 1000 s produced a bright rectangular area 5.5 μm wide in the SE image SEW (Fig. 3). CL imaging shows PDW and CDW of 5.5 and 3.5 μm, respectively. For both 30 and 60 kx, CDW was 2.0 μm. PDW was 3.5 and 3.0 μm at 30 and 60 kx magnification, respectively. At 120 kx, affected SEW was 2.5 μm, PDW-CL was 2.0 μm, and CDW-CL was 1.0 μm. Width of bright contrast in SEW decreased by 36% when the magnification was changed from 15 to 30 kx, by 16% when the magnification was changed from 30 to 60 kx, and by 20% when the magnification was changed from 60 to 120 kx. CDW decreased by 42% when the magnification was increased from 15 to 30 kx. CDW remained unchanged whether the magnification was 30 or 60 kx, and decreased by 50% when the magnification was increased from 60 to 120 kx. PDW in NBE-CL imaging was approximately the same as SEW up to 60 kx, where PDW decreased by 33% from 60 and 120 kx magnifications, and the results are plotted in Fig. 3. Calculated scan width at 15 kx, as provided by calibrated on-screen measurements (4.7 μm, and subsequently 2.3, 1.1, and 0.5 μm at increasing magnifications), are smaller than both SEW and PDW, as shown in Fig. 3.

These findings suggest that under extreme irradiation conditions (400 μW), sizes of affected regions seen by SE and CL do not scale with magnification and therefore are poor indicators of scanned region size in GaN despite interaction volume considerations. In fact, SEW at 15 kx is 0.8 μm larger than the calculated scan width, suggesting that at these irradiation settings, some of the contrast seen in SE imaging is the result of repulsion from injected electrons within the

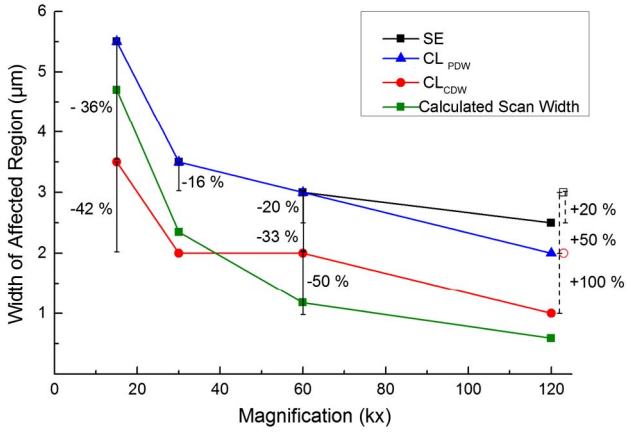

Fig. 3. Changes in width of degraded regions at different magnifications upon extreme irradiation. Black squares show SEW and blue triangles and red circles represent PDW (defined above) and CDW, respectively. These values were obtained upon 1000 s irradiation. The corresponding empty symbols and dashed lines show analogous measurements at 120 kx magnification when irradiated for 2000 s.

interaction volume. The calculated Kanaya–Okayama range at 20 keV in GaN is 2.2 μm [23].

It is worth highlighting the similar trends in SEW and PDW up to 60 kx, diverging at 120 kx. Also, there is some parallelism between SEW and CDW except at the 30–60 kx regime, where CDW remains unchanged and SEW becomes larger than the calculated scan width. These results suggest that dynamics of internal space charge region generation are complex.

Given the nonlinear dependence of SEW, PDW, and CDW with magnification, e-beam-induced processes with different energy barriers may be coming into play at different magnifications, i.e., when sufficient electrostatic energy density is available to the system. This is further confirmed by the five-fold increase at 120 kx magnification between the calculated scan width (0.5 μm) and SEW (2.5 μm), which is now of the same magnitude as the interaction volume. Contrary to arguments proposing metastable structural defects derived from doping as degradation agents [8], these results confirm the feasibility of e-beam damage of nominally undoped GaN, which had also been reported in nominally undoped zinc oxide (ZnO) [1].

B. Effects of Irradiation Time

Effects of prolonged extreme irradiation were examined at 120 kx by exposing a fresh area to continuous irradiation for 2000 s (Figs. 4 and 5). In this experiment, SEW was 3.0 μm whereas PDW and CDW were 3.0 and 2.0 μm, respectively. The affected area showed a 20% increase SEW, 50% increase in PDW, and 100% increase in CDW CL as compared with an irradiation time of 1000 s. These results are shown in Fig. 3 as open symbols and dashed lines.

Implications of SEW, PDW, and CDW being time-dependent are significant. They point at strong electric fields active beyond the irradiated region. Indeed, if SEW from 15 kx is taken as nominal scanned width, irradiation at 120 kx would

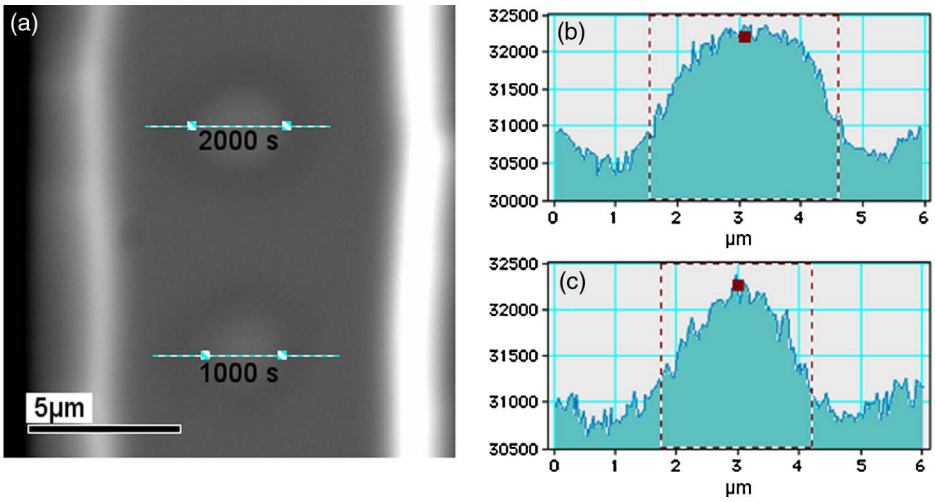

Fig. 4. (a) SEM image of two irradiated regions shown as bright spots at 120 kx magnification for 2000 s (top) and 1000 s (bottom), (b) Line profile intensity of SE of scanned region in the top. (c) Line profile intensity of SE of scanned region in the bottom.

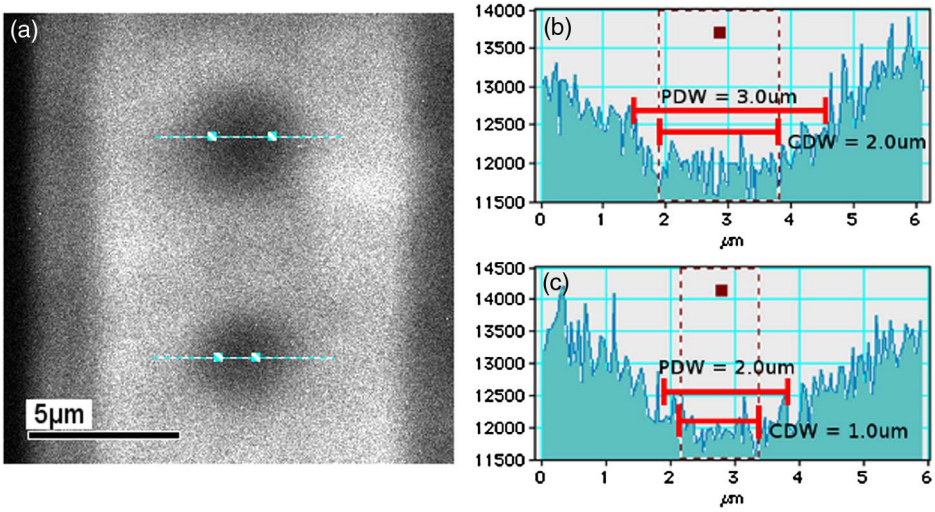

Fig. 5. (a) NBE-CL image of the same two irradiated regions in Fig. 4(a). Here, regions appear dark and show irradiation for 2000 s (top) and 1000 s (bottom). Also shown are the line profiles of CL intensity of the scanned region in the (b) top and (c) bottom images.

yield a SEW of 0.6 μm, which is a fraction not only of SEW at 1000 s (2.5 μm) but also smaller than CDW at 1000 s (1 μm), and certainly at 2000 s as well (2 μm). Time-based NBE-CL reports usually describe spectral data resulting from an integrated acquisition and do not correlate emissions with spatial distribution [6,8]. These results suggest that comprehensive modeling of electric field dynamics during extreme e-beam bombardment ought to take into account both the temporal and spatial effects of electric fields on CL emissions.

4. EFFECTS ON EXTREME AND MODERATE IRRADIATION CONDITIONS ON DL-CL EMISSION DISTRIBUTION AT DIFFERENT MAGNIFICATIONS

Contrary to the highly dynamical degradation processes observed in SE and NBE-CL, deep-level CL (DL-CL) images show identical contrast between irradiated and nonirradiated regions at all magnifications. The DL-CL image in Fig. 6 was acquired in the same region as Fig. 2(a), where the (extreme) irradiation experiments at 30 kx magnification decreased NBE-CL intensity. The DL-CL image in Fig. 6 does not show any intensity difference in the scanned region compared to the adjacent pristine regions, contrary to observations by Pozina [8], which identified interplay between acceptor-bound exciton emissions and recombinations at prismatic stacking faults (PSFs) by low-temperature t-CL. In fact, PSFs were found to develop under e-beam irradiation, further affecting recombination of donor–acceptor pairs [8].

Absence of variations in DL emissions, in our case, leads to several conclusions. First, electrostatic effects promoted by irradiation do not alter the distribution of impurity recombination sites—through electromigration, for example. Second, since time-dependent DL-CL (not shown) is constant, and the recombination efficiency of DL centers (recently attributed to C_N in addition to the well-established V_{Ga} [24]) have not been affected by charge dynamics. Finally, CL wavelength scans acquired after irradiation (not shown) lack additional emissions other than NBE and DL. These results suggest that the optical energy lost during time-dependent NBE-CL is likely to be invested in phonon-assisted processes, leading to nonradiative recombination. Whether e-beam damage may be nucleating these interband states is unclear at this point, and will be further discussed in Section 5.A. Similarly, irradiation under moderate conditions did not show any time- or spatial-resolved variations in DL-CL. The effects of moderate irradiation conditions on NBE-CL will be discussed in the next section.

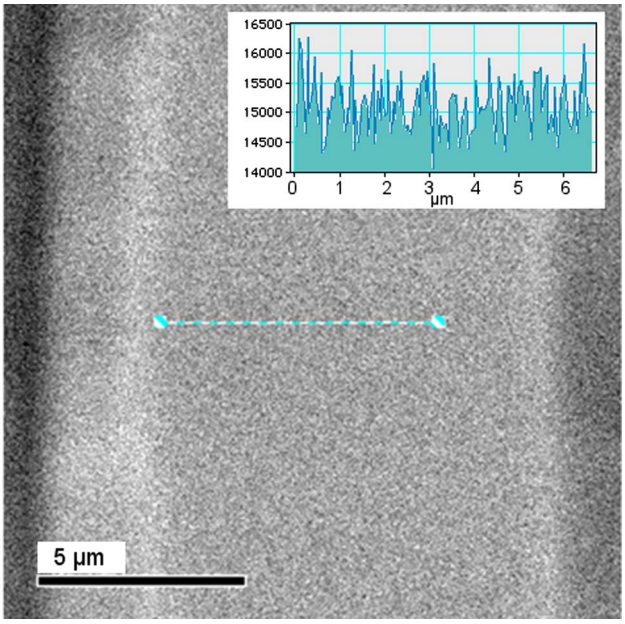

Fig. 6. DL-CL image of region upon irradiation at extreme conditions (30 kx, 1000 s), revealing no contrast difference between irradiated and nonirradiated regions. The inset shows a DL-CL profile across the unaffected irradiated region.

5. SPACE CHARGE REGION BUILDUP AND CL DYNAMICS UNDER MODERATE IRRADIATION CONDITIONS

A. Dynamic Evolution of NBE-CL and SC Correlated with SE Emissions: Effects of Adsorbed States

By attaching carbon-tape stripes from the sample to the specimen holder, the conductive coating layer on GaN was effectively grounded. This simple setup readily facilitates a suitable electrical path to ground that enabled *in situ* SC measurements. The interplay between SC, NBE-CL, and SE emissions was addressed by conducting simultaneous CL and SC *in situ* moderate irradiation experiments at 10 μW, with 15 and 30 kx magnifications. The comparative discussion between NBE-CL and SC in the different scenarios revolves around times to reach steady state and the nature of SC contributions. Indeed, SC resulting from e-beam irradiation has been previously modeled as the sum of two contributions [25], displacement (i_d) and leakage (i_l) currents:

$$i_{SC} = i_d + i_l = \frac{Q(\infty)}{\tau'} e^{-t/\tau'} + \frac{g_i}{\varepsilon_o \varepsilon_r} Q(\infty)(1 - e^{-t/\tau'}), \quad \textbf{(1)}$$

where $Q(\infty)$ is the total injected charge at steady state, τ' is a time constant resulting from the exponential fit, ε_0 and ε_r are dielectric constants of vacuum and GaN, respectively, and g_i is bombardment-induced conductivity [25].

Irradiation at 15 kx produced a rapidly decaying CL curve and a smoothly decaying SC curve with times to steady states of 600 and 900 s, respectively [Fig. 7(a)]. Compared with t-CL at 15 kx, irradiation at 30 kx yielded steady states at 400 s (CL) and 800 s (SC), as seen in Fig. 7(b). In this scenario, irradiated regions showed increased SE emission upon irradiation (inset, Fig. 7). It is worth highlighting that the presence of both terms is a definite indication of charge trapping upon irradiation. Indeed, both i_d and i_l contributions are present in SCs, which reveal negative charge storage upon irradiation—consistent with increased SE—as a result of repulsion from incoming electrons [25,26]. Similar irradiation experiments were conducted immediately after exposing the GaN on sapphire (GaN/Al_2O_3) wafer to ambient humidity (Fig. 8). In this discussion, we will refer to both experimental conditions as humidity desorbed and absorbed scenarios (HDS and HAS), respectively, since humidity-related adsorption and desorption

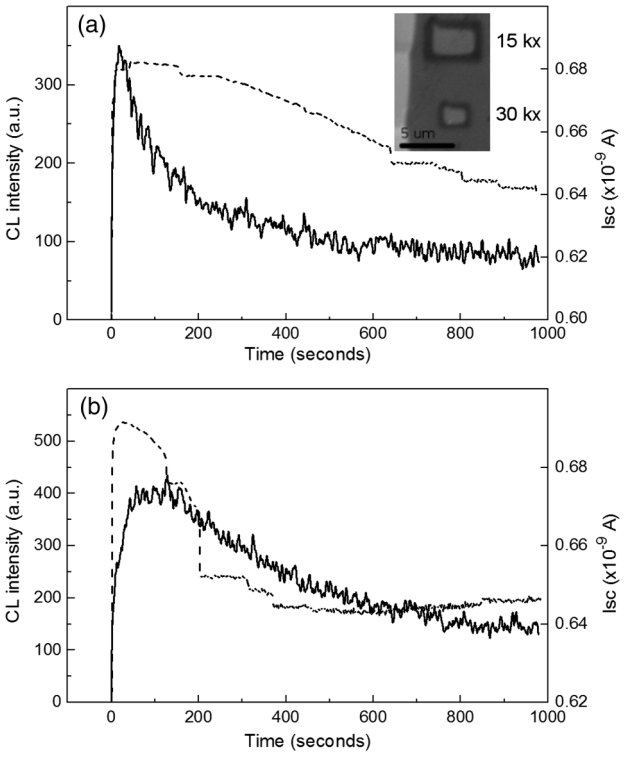

Fig. 7. Time-dependent NBE-CL (solid lines) and SC (dashed lines) measurements of HDS acquired at (a) 15 kx magnification and (b) 30 kx magnification. Inset shows SEM image of irradiated regions as bright rectangles at 15 and 30 kx magnification.

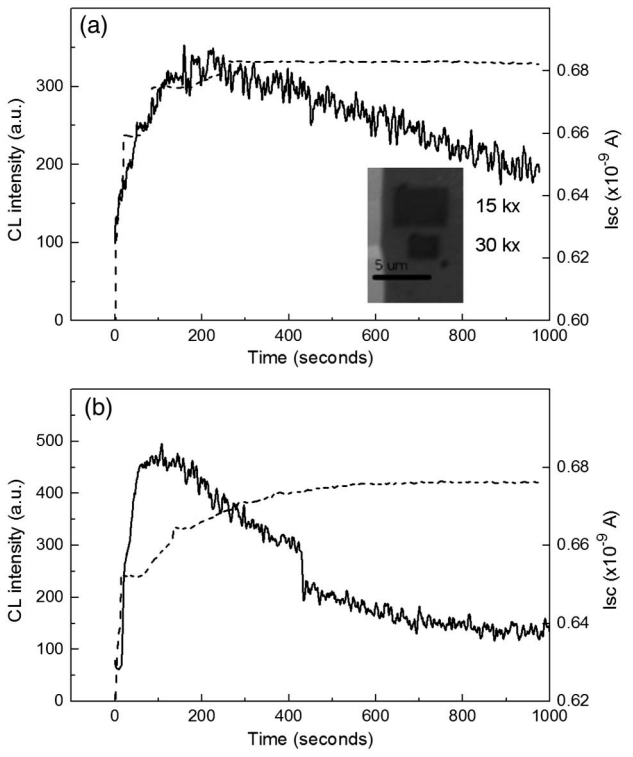

Fig. 8. Time-dependent NBE-CL (solid lines) and SC (dashed lines) measurements of HAS at (a) 15 kx and (b) 30 kx magnification. Inset shows SEM image of irradiated regions as dark rectangles.

are likely responsible for these scenarios as previously highlighted in the introduction.

Interestingly, in HAS, irradiation at 15 kx produced slowly increased CL and SC curves during initial irradiation stages [Fig. 8(a)]. At 30 kx, CL initially increased [Fig. 8(b)] as in HDS [Fig. 7(b)]; however, SC retained the same dynamics of irradiation as in 15 kx in HAS [Fig. 8(b)]. In conclusion, HAS has relented CL degradation dynamics and drastically modified contributions to SC. Indeed, the exponentially increased SC correlates with an exclusive contribution from leakage current i_l in the absence of charge trapping and therefore yields reduced SE contrast since no charge will be injected, according to Song's model [25], where the SC seen in HAS represents leakage current only. Albeit despite the dual contribution to SC ($i_d + i_l$) in HDS and the single contribution (i_l) in HAS, the resulting NBE-CL at 30 kx are surprisingly similar, with times to steady state SC of ~400 s and final CL intensities of ~125 a.u. in both cases. These results suggest that a multiplicity of internal field dynamics can provide identical NBE-CL time profiles, even in the absence of injected charges.

One of the most remarkable results in this work is the disparity in SE and t-CL emissions from HDS and HAS, suggesting that the environmental history of GaN is relevant to optoelectronic phenomena by way of surface effects [1,6]. There are two possible mechanisms responsible for the decreased contrast observed in SE images, which is feasible if we consider a residual humidity layer on the irradiated surface. The proposed mechanisms are either through shielding of SE due to a positive surface charge [6], or through migration of H^+ ions to the GaN promoted by e-beam irradiation [27,28], In HDS, charge is being injected into the interaction volume ($SC = i_d + i_l$) until a saturation level is reached and therefore a bright SEM contrast image is produced. This is due to the repulsion of incoming electrons to the already electron-rich interaction volume. In HAS, charge is being accelerated into a volume whose internal fields are shielded by the positively charged adsorbed layer (upon ionization from the e-beam), tailoring the SC to avoid charge injection ($SC = i_l$), and yielding intense leakage currents [25].

Built-in charge density greatly affects carrier recombination dynamics. Indeed, times to steady state are greatly altered by surface adsorption since ionized water molecules are known to modify charging characteristics of GaN devices at the nanoscale [6]. However, charging dynamics, as shown by the SC curves, reveal that HAS only contributes to SC with i_l. HDS contributes to SC with both i_l and i_d, the former allowing for transient charge trapping/detrapping processes and the latter conducive to charge injection. Surprisingly, i_l alone can already affect NBE-CL [Fig. 8(b)], even with the same efficiency as i_d [Fig. 7(b)]. Due to electronegativity differences between the Ga and N sublattices, a spontaneous polarization exists along the c axis in GaN. Thomsen [18] showed that a surficial layer of positive ions, or charged particles picked up from the air, were sufficient in screening the polarizing field. Upon desorption, polarization is descreened and an electric field is set up which promotes electron hole pair separation. This is consistent with our findings, where the absence of an adsorbed layer effectively

contributes to the modulation of NBE CL. Unlike Thomsen, however, we find that charge was stored in the volume upon e-beam irradiation, further increasing internal field strength.

The interplay between spontaneous polarization field, electric field buildup as a result of injected charge, and V_{Ga} activation is unclear at this time. However, we can make important predictions on the chemistries of defects behind decreased NBE-CL and the ubiquitous DL-CL in our samples. Indeed, given the high scanning rates used in these experiments, current densities in our study (30 $kAcm^{-2}$) are comparable to those reported by Nykänen *et al.* [13] (and hence comparable to device operative conditions), who correlated the activation of V_{Ga} (from V_{Ga} – 3H complexes) with decreased NBE emissions. Reportedly, the activation mechanism could be either through electron energy transfer, current density, or both. Although our study does not help to fully clarify the activation mechanism, our findings suggest that if V_{Ga} are solely responsible for the decreased NBE, their activation does not require charge injection [25], as seen in Fig. 8, and current density from leakage could suffice to promote activation. In addition, if V_{Ga} are activated upon irradiation, their contribution to DL emissions in these MOCVD-grown LEO films is negligible given the lack of variation in DL-CL as seen in Fig. 6, suggesting C_N as suitable candidates [24]. Damage permanence has been confirmed through a minimum 48-h period where the bombarded regions were kept at high vacuum and room temperature. Damage persistence could further support the V_{Ga} activation model, albeit stability of V_{Ga} versus V_{Ga} – 3H complexes, either under vacuum or under more diverse physicochemical environments, is unclear at this time.

It is worth emphasizing that CL is an especially suitable technique to address recombination dynamics affected by surface states. In fact, the sampling depth in CL can be optimized toward surface sensitivity. Upon correction from self-absorption, NBE emission in GaN is collected from within the first 1000 nms of the surface at 20 kV, although only within 500 nms at 10 kV, yielding a distribution maxima at 125 nm [29] and emphasizing the contribution of surface states. Surface states in GaN have shown large impact in their CL fingerprint. Indeed, Dierre *et al.* [1] found that NBE-CL signal could either increase or decrease upon t-evolved e-beam irradiation as a function of surface termination. In fact, the suitability adsorbed surface species (molecular oxygen and water) to strongly modify time-dependent luminescence at room temperature has been confirmed recently [30].

The study of t-CL in different environmental conditions goes beyond an academic curiosity since t-CL dynamics offer a window into optoelectronic device efficiency, with evidence of humidity effects on NBE-CL signal evolution having been reported earlier [6]. Indeed, Wang *et al.* reported higher intensity and faster NBE degradation from environmentally exposed GaN. Contrary to their report, we found similar NBE intensities and slower decay in HAS than HDS. In fact, the NBE-CL degradation was attributed to the desorbing action of Van der Waals-bonded humidity molecules. In addition, it is precisely in HDS where the NBE-CL degradation is stronger, in clear contradiction with the proposed phenomenology albeit our data further confirms surface adsorbed states do play an important role in charge dynamics and consequently in NBE-CL. Lastly, the dual SE contrast as a function of environmental conditions further supports the notion that the occasional observation of decreased SE contrast upon irradiation is not due to the deposition of a carbonaceous contamination layer [7].

B. Diode Model: Effects of Electron Beam Irradiation and Surface Adsorbed States on NBE-CL

Charging under e-beam influence is a highly dynamic process and models have been attempted earlier [25,31]. Two fields must be considered to understand behavior of charges within the systems, derived from the two contributions to SC introduced earlier. First, a nominal electric field which results from excess charges in the slightly n-type GaN, which is responsible for drift of charge carriers that conform i_l. Second, a built-in field due to injected charge from the e-beam as a consequence of i_d. Therefore, total field upon irradiation is equal to nominal field plus built-in field.

Initially, our proposed phenomenological model, featuring an environmentally derived adsorbed layer, agrees with previous reports that emphasize the impact of water adsorption on electric charge transport at the Nanoscale [30], and the feasibility of physisorbed O_2 to quench Si nanoparticle luminescence at room temperature [30]. Furthermore, humidity has reportedly produced deleterious effects on organic thin film transistors [32]. The feasibility of the proposed mechanism has been demonstrated earlier, through diffusion of ionic hydrogen through metal/GaN contacts, leading to Schottky barrier height (SBH) reduction through the generation of a dipole layer and causing a shift in the relative electrostatic potential of GaN [28] and work function of the Au contact [27]. These results indicate that, at least under adequate irradiation conditions, nominal fields suffice to alter NBE-CL during continued e-beam bombardment, as seen in Fig. 8. In fact, nominal fields [Fig. 8(b)] can be as efficient as built-in fields [Fig. 7(b)] in modifying NBE-CL. The dynamics of the internal charge trapping and beyond will be discussed through a model in terms of band bending in this next section.

Variability observed here in HDS and HAS points at an interplay of internal fields promoting band bending and changing depletion width (DW) at the Au/GaN interface, prone to 2D diode modeling. A comprehensive understanding of the effects of humidity adsorption on electron-beam sample interaction requires a detailed description of deposited Au on GaN. However, controversy exists surrounding the exact behavior at the Au/GaN interface, and the presence of a thin oxide layer has been reported as a defining factor [33]. The exact nature of interface interactions is not fully understood, with reports of both Ga [34] and N [35] diffusing into Au contacts and Au/n-GaN becoming ohmic upon annealing [36]. In addition, work functions (φ) of GaN and atomically clean Au are 4.1 [37] and 5.2 eV [38], respectively, and a value as low as 4.3 eV has been reported in Au upon thermal evaporation [38]. Albeit, despite large variety of factors determining barrier type [33,37,39], Au deposited at room temperatures will form a Schottky barrier to n-GaN [36]. This contact favors charge movement from semiconductor to metal, but is highly resistive to reverse current. Highly rectifying contacts [34] have been

attributed to the formation of an Au/AuN_x layer at the contact interface [35].

1. HDS 2D Diode Model

In HDS, the Au/GaN wafer was kept under vacuum for over 24 h. During this period, residual humidity from ambient exposure will have desorbed and surface passivation quenched [6]. Nominally undoped GaN is slightly n-type and therefore electron rich [40]. Upon initial irradiation, HDS n-GaN will build up charge within the interaction volume [$SC = i_d + i_l$ in Fig. 7(a)], which will repel further incoming electrons, leading to increased backscattering and a bright SEM image (inset in Fig. 7). Electrons will diffuse to the contact because of the carrier density gradient promoted by the built-in field. This favors movement of electrons through the surface, a path of least resistance versus the bulk, where defects offer a greater resistance [40]. A rectifying contact exists at the Au/GaN interface, and because of injected energy, electron migration to ground is favored. In this scenario, the Schottky barrier height (SBH_a) is high [Fig. 9(a)], and energy must be supplied to each electron to overcome this barrier, i.e., to overcome trapping, which in turn enhances SE emissions. With increasing negative charge at the contact, a depletion layer of trapped holes [Fig. 9(a)] is generated in GaN, where there is little opposition to the depletion, yielding a wide depleted region (DW_a) in HDS. As a consequence, CL is initially intense [Fig. 7(a)] due to excess electrons in the interaction volume, yielding high probability of recombination. Over time, recombination events will decrease as more electrons are trapped and luminescence degrades due to the increasingly established built-in field which is now opposing electron-hole recombination. The initial exponential decrease in CL observed here is also consistent with nonradiative recombinations via surface defects recently reported in GaAs [41].

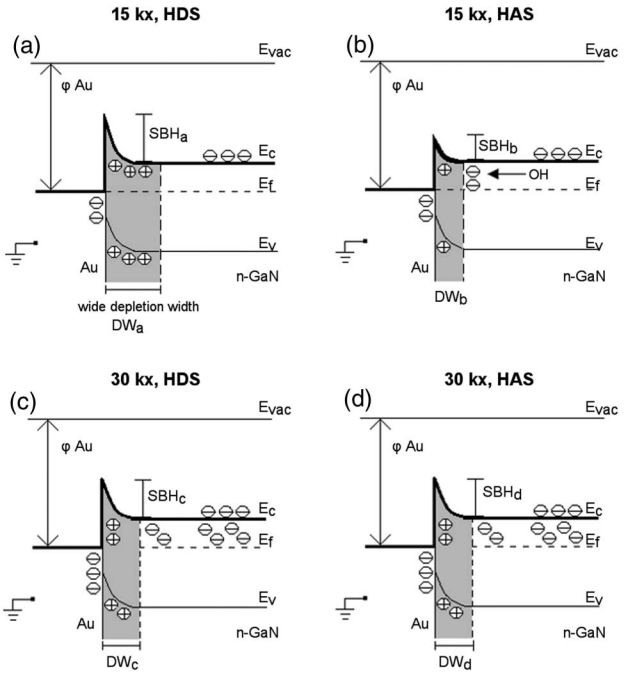

Fig. 9. (a) HDS, 15 kx magnification, when DW and SBH are large. (b) HAS 15 kx; ionized water affects SBH and DW. (c) HDS 30 kx; built-in field lowers SBH and DW. (d) HAS 30 kx; built-in field increases SBH and DW from (b).

2. HAS 2D Diode Model

In HAS (Fig. 8), GaN was purposefully exposed to ambient and immediately irradiated. There is evidence to suggest that water molecules present at the surface of a semiconductor can be ionized in the presence of an electric field, leaving the surface slightly positively charged [$H_2O > e^- + H^+ + OH^\cdot$] [30,42]. As discussed earlier, in HAS, positive surface charge is held by free electrons in n-GaN, which accelerates incoming beam electrons into the interaction volume, inhibiting SE emissions and leading to a dark contrast in SEM [inset Fig. 8(a)]. However, upon continuous e-beam irradiation, these further-injected charges drift to the contact; they do not become trapped [$SC = i_l$ in Fig. 8(a)]. Schottky barrier potential is reduced (SBH_b) by the influence of H^+ ions [Fig. 9(b)] [27,28], favoring transport of electrons to ground. Upon initial SC increase, when the nominal field has not been established, NBE-CL is seen to increase as well. However, upon nominal field establishment, electron-hole pairs are separated [NBE-CL decreases in Fig. 8(a)], with electrons being accelerated toward the contact [increased SC at steady state in Fig. 8(a)].

As the contact becomes slightly negative, a depletion region (DW_b) of fixed holes forms at the AuGaN interface [Fig. 9(b)]. This is opposed by the presence of free electrons and $OH^\cdot$ radicals and therefore is narrow compared with scenario shown in Fig. 9(a). SC steady state is reached after ~300 s, suggesting that drift charge is balanced by repulsive influence of the negative contact which sets up DW_b. Both CL and SC increase concurrently to their respective maximum values after ~200 s. As DW is formed, CL then decreases to a steady state at around 900 s whereas SC remains steady from 200 s. As charge is not trapped within the volume, NBE-CL is intense owing to unaffected (radiative) electron hole pair recombination. A positive surface potential causing band bending and screening incident electrons is combined with a depletion layer at the contact, which repels free holes. Free charges within the sample could be enhancing recombination efficiency of electron hole pairs generated by the e-beam. This is consistent with Lagemaat's findings [43], where enhanced photoemission was seen upon electron hole pair generation in regions beyond the contact diffusion length [1,43]. In effect, nominal leakage current leads to a narrow DW [Fig. 9(b)], whereas charge trapping and displacement current cause a wider DW [Fig. 9(a)].

C. Dynamic Evolution of SC and CL at Higher Magnification

At 15 kx magnification, CL and SC dynamics seen in HDS and HAS differ greatly. At 30 kx, however, CL evolution shows initial increase and then slow decay in both HDS and HAS. SC reaches steady state at ~400 s in both systems, but with opposite charging. This suggests that internal field greatly affects dynamics of charge carriers within the volume because built-in field density appears to have little influence on CL above a certain threshold. It is feasible that the nominal internal field is strong enough to affect recombination rates within GaN as much as a built-in field. This can be seen as a change in time to steady state, when magnification is increased from

15 to 30 kx. The effect of introducing excess negative charge to GaN by increasing magnification will alter the SBH at Au/GaN contact [Figs. 9(c) and 9(d)].

Steady state current (I_{ss}) shows a small variation with magnification. For HDS, I_{ss} increases from ~0.642 to ~0.648 nA. HAS shows a decrease in Iss from ~0.682 down to ~0.678 nA. For the case of HDS, irradiation at 30 kx has taken the system beyond a charging threshold, steady state is reached more quickly, and current is higher; this is consistent with a decreased depletion width (DW_c) and reduction in SBH [SBH_c, Fig. 9(c)]. A greater built-in field in the interaction volume will oppose widening of DW_c.

Conversely, increasing time constant and reduced current seen for the HAS [Fig. 9(d)] suggests a wider depletion region and SBH increase (DW_d and SBH_d, respectively). These results show that band bending and depletion widths have become similar in both HDS and HAS as the built-in field is increased by doubling magnification. Dynamics of SC must, therefore, be influenced by charge trapping within the interaction volume.

D. SBH Estimates from Thermionic Field Emission Theory

From experimental data, a model was attempted in the prior sections to explain observed effects through band bending at a rectifying metal–semiconductor contact. In this scenario, samples were treated as Schottky diodes operating within the standard operation conditions, away from avalanche breakdown. Band bending was then modeled as a function of differences in material work function and electron affinity, including a depleted charge region. This phenomenology is well known in device semiconductor physics, and has been quantitatively described through Thermionic Field Emission (TFE), a well-established theory in silicon technology [35]:

$$i_S = \mathrm{SA} * * T^2 \exp\left(\frac{-q\varphi_b}{KT}\right). \quad (2)$$

To further build upon the operating-diode model, SBH values [i.e., φ_b band bending at contact interface in Eq. (2)] were calculated from the TFE equation, where saturation current (i_s) was taken to be steady state SC and device surface area S was the affected area by the e-beam. The rest of the parameters in the equation, A, T, q, and K, are the well-known effective Richardson's constant (26 $A/m^2 K^2$ for GaN [33]), absolute temperature (298 K), electron charge, and Boltzmann's constant, respectively. Assuming Schottky diode formation and TFE as main current contribution, quantitative analysis of contact formation (Table 1) provided SBH in all four scenarios. In this derivation, S was taken to be the affected region found by analysis of SE, as shown earlier (inset Figs. 7 and 8).

Results in Table 1 reveal that values of SBH did not follow trends described by HDS and HAS models. A reduction in band bending occurs in HDS from 15 to 30 kx magnification, consistent with experimental observations; however, HAS show lower values of SBH with increasing magnification, contradicting both our experimental results as well as previous studies [27,28]. TFE theory is an unsuitable method for analyzing charge-dynamic behavior of GaN in these scenarios, due ultimately to multiple defects present in the plane of irradiation. Indeed, silicon has a highly ordered crystal lattice and well-understood defect centers can be tightly controlled. However, defect sites within GaN are not well understood and result in a nonuniform charge distribution within the interaction volume. These findings suggest that existing defects within the GaN affect not only charge distribution, but can also alter charging and recombination dynamics by way of power density variations.

Table 1. Calculated Values of SBH using TFE Theory Method

Schottky Barrier Height	HDS[a]	HAS
15 kx magnification	260.04×10^3 [6.88]	274.65×10^3 [12.92]
30 kx magnification	230.18×10^3 [2.17]	244.87×10^3 [4.02]

[a]Sample area parameter S in Eq. (2) is given for each case in square brackets with units pm^2 ($\times 10^{-12}$ m^2).

6. CONCLUSIONS

The effects of extreme and moderate e-beam irradiation of GaN exposed to different environments have been examined by SE, SC, and CL. For the first time to our knowledge, an integrated discussion considering surface effects, defect generation (by way of V_{Ga} activation), as well as internal field dynamics during electron beam bombardment has been presented.

We have identified two regimes where irradiation effects are either confined to or extend beyond nominal regions. Under extreme irradiation, the size of NBE-CL completely degraded regions does not vary linearly with magnification. Sizes of partially degraded regions are approximately the same as sizes of affected regions seen by SE imaging. Contrast seen in SE is attributed to electron irradiation and not to luminescent absorption effects through residual layers. Moreover, prolonged irradiation contributed to augmenting the size of SE- and CL-affected regions. Remarkably, DL luminescence remained unaffected under extreme and moderate irradiation. If indeed the activation of V_{Ga} is responsible for decreased NBE intensities, the centers responsible for DL emissions in these films are possibly C_N. These results also suggest that electromigration of C_N centers has not been promoted, and that their recombination efficiency is not affected by either trapped or injected charges.

For the first time to our knowledge, *in situ* monitoring of NBE and SC measurements upon electron beam irradiation has been conducted in GaN, producing a phenomenologistic band-bending model at the Au/GaN interface. Under moderate irradiation environments, two scenarios were identified taking into account sample handling, and the presence of a humidity layer has been predicted. Indeed, upon reduced vacuum exposure, all SE contrast, time-dependent SC, and CL revealed characteristic trends that are attributed to the presence of a surface humidity layer which could be affecting electrostatic dynamics. We have presented a 2D diode to model time-dependent NBE-CL, where the evolution of CL can be provided exclusively as a function of electrostatic fields during

device operation. The model can explain SC and CL dynamics through band bending. In this scheme, Schottky barrier heights and depletion widths develop and evolve as a function of internal fields, either nominal (through leakage currents from trapped charges in shallow states) or through additional built-in field (contributing an additional displacement current from injected charges in deep states). Variations on irradiation conditions (magnification) and available surface states (as they pertain to humidity sorption) effectively modify diode parameters to correlate with SC, SE, and CL evolution. Good agreement between the proposed 2D diode model and experimental findings offers evidence of the presence of a surficial adsorbed layer in the one scenario. Leakage and displacement currents are correlated with trapped and injected charges, respectively. We found that leakage currents alone can efficiently alter the evolution of NBE-CL, suggesting that transient fields promoting trapping–detrapping during device operation readily affect NBE-CL in the absence of injected charge in deep states. TFE theory was found unsuitable to quantify the proposed model, owing to the uncertain role of nonluminescent GaN defects on charge distribution and recombination dynamics.

Our findings agree with prior reports on the importance of surface recombination in CL; however, desorption processes are not exclusively responsible for NBE-CL evolution, since stronger degradation is observed in absence of surficial layers. Conversely, weaker NBE-CL degradation corresponds to a low irradiation dose with a positive surficial charge, such as that provided by a residual humidity layer.

Future work will further explore the correlation between irradiation conditions and CL dynamics, to elucidate whether V_{Ga} are activated upon knock-on damage or through current density effects. As we have discussed previously, this elucidation may validate t-CL as a predictor of degradation in GaN devices.

The authors gratefully acknowledge scientific discussions with G. Slade Cargill III.

REFERENCES

1. B. Dierre, X. Yuan, and T. Sekiguchi, "Low-energy cathodoluminescence microscopy for the characterisation of nanostructurres," Sci. Tech. Adv. Mater. **11**, 1–10 (2010).
2. K. J. Lethy, P. R. Edwards, W. N. Wang, and R. W. Martin, "Cross-sectional and plan-view cathodoluminescence of GaN partially coalesced above nanocolumn array," J. Appl. Phys. **112**, 023507 (2012).
3. S. Nakamura and G. Fasol, *The Blue Laser Diode: GaN based Light Emitters and Lasers*, 2nd ed. (Springer, 1997), p. 343.
4. S. J. Pearton, ed. *GaN and Related Materials, Optoelectronic Properties of Semiconductors and Super Lattices* (Gordon and Breach, 1997), Vol. **2**, p. 85.
5. J. Neugebauer and C. G. Van de Walle, "Gallium vacancies and the yellow luminescence in GaN," Appl. Phys. Lett. **69**, 503–505 (1996).
6. Y. Wang, B. Dierre, T. Sekiguchi, Y. Z. Yao, X. L. Yuan, F. J. Xu, and B. Shen, "Surface effects on the luminescence degradation of hydride vapor-phase epitaxy-grown GaN induced by electron-beam irradiation," J. Vac. Sci. Technol. A **27**, 611–613 (2009).
7. E. M. Campo, G. S. Cargill III, M. Pophristic, and I. Ferguson, "Electron beam bombardment induced decrease of cathodoluminescence intensity from GaN not caused by absorption in buildup of carbon contamination," MRS Internet nitride Semicond. Res. **9**, 8 (2004).
8. G. Pozina, P. P. Paskov, J. P. Bergman, C. Hemmingsson, L. Hultman, and B. Monemar, "Metastable behavior of the UV luminescence in Mg-doped GaN layers grown on quasibulk GaN templates," Appl. Phys. Lett. **91**, 221901 (2007).
9. E. J. Vesseur, T. Coenen, H. Caglayan, N. Engheta, and A. Polman, "Experimental verification of n = 0 structures for visible light," Phys. Rev. Lett. **110**, 013902 (2013).
10. C. I. Pakes, J. A. Garrido, and H. Kawarada, "Diamond surface conductivity: properties, devices, and sensors," MRS Bull. **39**, 542–548 (2014).
11. P. Sherwood, "Charging issues in electron spectroscopies," J. Electron Spectrosc. Relat. Phenom. **176**, 2–4 (2010).
12. M. Meneghini, S. Carraro, G. Meneghesso, N. Trivellin, G. Mura, F. Rossi, G. Salviati, K. Holc, T. Weig, L. Schade, M. A. Karunakaran, J. Wagner, U. T. Schwarz, and E. Zanoni, "Degradation of InGaN/GaN laser diodes investigated by micro-cathodoluminescence and micro-photoluminescence," Appl. Phys. Lett. **103**, 233506 (2013).
13. H. Nykänen, S. Suihkonen, L. Kilanski, M. Sopanen, and F. Tuomisto, "Low energy electron beam induced vacancy activation in GaN," Appl. Phys. Lett. **100**, 122105 (2012).
14. H. Nykänen, S. Suihkonen, T. Tanikawa, M. Yamaguchi, Y. Honda, and H. Amano, "Effects of low energy e-beam irradiation on cathodoluminescence from GaN," Phys. Status Solidi A **210**, 383–385 (2013).
15. A. Y. Polyakov, D. W. Jeon, I. H. Lee, N. B. Smirnov, A. V. Govorkov, E. A. Kozhukhova, and E. B. Yakimov, "Electrical properties of undoped GaN films grown by maskless epitaxial lateral overgrowth," J. Appl. Phys. **113**, 083712 (2013).
16. A. M. Fischer, S. Srinivasan, F. A. Ponce, B. Monemar, F. Bertram, and J. Christen, "Time-resolved cathodoluminescence of Mg-doped GaN," Appl. Phys. Lett. **93**, 151901 (2008).
17. M. A. Reshchikov and H. Morkoc, "Luminescence properties of defects in GaN," J. Appl. Phys. **97**, 061301 (2005).
18. M. Thomsen, H. Jönen, U. Rossow, and A. Hangleiter, "Effects of spontaneous polarization on GaInN/GaN quantum well structures," J. Appl. Phys. **109**, 123710 (2011).
19. L. Hussey, S. Mita, J. Xie, W. Guo, C. R. Akouala, J. Rajan, I. Bryan, R. Collazo, and Z. Sitar, "Lateral epitaxial overgrowth of nitrogen polar GaN on smooth nitrogen polar GaN templates by metalorganic chemical vapor deposition," J. Appl. Phys. **112**, 113513 (2012).
20. N. Rastgar, D. J. Rowe, R. J. Anthony, B. A. Merritt, U. R. Kortshagen, and E. S. Aydil, "Effects of water adsorption and surface oxidation on the electrical conductivity of silicon nanocrystal films," J. Phys. Chem. C **117**, 4211–4218 (2013).
21. T. George, K. A. Son, R. A. Powers, L. Y. Del Castillo, and R. Okojie, "Harsh environment microtechnologies for NASA and terrestrial applications," in *Sensors, 2005 IEEE*, (IEEE, 2005).
22. K. A. Son, A. Liao, G. Lung, M. Gallegos, T. Hatake, R. D. Harris, L. Z. Scheick, and W. D. Smythe, "GaN-based high-temperature and radiation-hard electronics for harsh environments," Proc. SPIE **7679**, 76790U (2010).
23. M. Suzuki, K. Kumagai, T. Sekiguchi, A. M. Cassell, T. Saito, and C. Y. Yang, "Secondary electron emission from freely supported nanowires," J. Appl. Phys. **104**, 114306 (2008).
24. J. L. Lyons, A. Janotti, and C. G. Van de Walle, "Carbon impurities and the yellow luminescence in GaN," Appl. Phys. Lett. **97**, 152108 (2010).
25. Z. G. Song, C. K. Ong, and H. Gong, "A time-resolved current method for the investigation of charging ability of insulators under electron beam irradiation," J. Appl. Phys. **79**, 7123–7128 (1996).
26. J. Cazaux, "Secondary electron emission and charging mechanisms in auger electron spectroscopy and related e-beam techniques," J. Electron Spectrosc. Relat. Phenom. **176**, 58–79 (2010).
27. J. Kim, F. Ren, B. P. Gila, C. R. Abernathy, and S. J. Pearton, "Reversible barrier height changes in hydrogen-sensitive Pd/GaN and Pt/GaN diodes," Appl. Phys. Lett. **82**, 739 (2003).
28. J. Schalwig, G. Muller, U. Karrer, M. Eickhoff, O. Ambacher, and M. Stutzmann, "Hydrogen response mechanism of Pt–GaN Schottky diodes," Appl. Phys. Lett. **80**, 1222 (2002).
29. K. Fleischer, M. Toth, M. R. Phillips, J. Zou, G. Li, and S. J. Chua, "Depth profiling of GaN by cathodoluminescence microanalysis," Appl. Phys. Lett. **74**, 1114–1116 (1999).
30. M. J. Llansola Portolés, P. M. Gara, M. L. Kotler, S. Bertolotti, E. San Román, H. B. Rodríguez, and M. C. Gonzalez, "Silicon nanoparticle photophysics and singlet oxygen generation," Langmuir **26**, 10953–10960 (2010).

31. J. Cazaux, "Some considerations on the secondary electron emission, δ, from e–irradiated insulators," J. Appl. Phys. **85**, 1137–1147 (1999).
32. D. Li, E. J. Borkent, R. Nortrup, H. Moon, H. Katz, and Z. Bao, "Humidity effect on electrical performance of organic thin-film transistors," Appl. Phys. Lett. **86**, 042105 (2005).
33. X. J. Wang and L. He, "Electrical characteristics of high performance Au/n-GaN Schottky diodes," J. Electron. Mater. **27**, 1272–1276 (1998).
34. K. Wang, R. X. Wang, S. Fung, C. D. Beling, X. D. Chen, Y. Huang, S. Li, S. J. Xu, and M. Gong, "Film thickness degradation of Au/GaN Schottky contact characteristics," Mater. Sci. Eng. B **117**, 21–25 (2005).
35. N. Spyropoulos-Antonakakis, E. Sarantopoulou, Z. Kollia, Z. Samardzija, S. Kobe, and A. C. Cefalas, "Thermionic field emission in gold nitride Schottky nanodiodes," J. Appl. Phys. **112**, 094301 (2012).
36. J. S. Foresi and T. D. Moustakas, "Metal contacts to gallium nitride," Appl. Phys. Lett. **62**, 2859–2861 (1993).
37. S. J. P. F. Ren and M. O. Manaresh, *GaN and Related Materials, optoelectronic Properties of Semiconductors and Superlattices* (Gordon and Breach, 1997), Vol. **2**.
38. S. Scheinert, M. Grobosch, J. Sprogies, I. Horselmann, M. Knupfer, and G. Paasch, "Organic [6,6]-phenyl-C61-butyric-acid-methyl-ester field effect transistors: analysis of the contact properties by combined photoemission spectroscopy and electrical measurements," J. Appl. Phys. **113**, 174504 (2013).
39. L. Wang, F. M. Mohammed, and I. Adesida, "Differences in the reaction kinetics and contact formation mechanisms of annealed Ti/Al/Mo/Au Ohmic contacts on n-GaN and AlGaN/GaN epilayers," J. Appl. Phys. **101**, 013702 (2007).
40. T. L. Tansley, E. M. Goldys, M. Godlewski, B. Zhou, and Y. Zuo, *The Contribution of Defects to the Electrical and Optical Properties of GaN, Optoelectronic Properties of Semiconductors and Superlattices* (Gordon and Breach, 1997), Vol. **2**.
41. D. Sager, C. Gutsche, W. Prost, F. J. Tegude, and G. Bacher, "Recombination dynamics in single GaAs-nanowires with an axial heterojunction: n- versus p-doped areas," J. Appl. Phys. **113**, 174303 (2013).
42. E. Rowicka, D. Kashyn, M. A. Reagan, T. Hirano, P. B. Paramonov, I. Dolog, R. R. Mallik, and S. F. Lyuksyutov, "Influence of water condensation on charge transport and electric breakdown between an atomic force microscope tip, polymeric, and (Semiconductor) CdS surfaces," Curr. Nanosci. **4**, 166–172 (2008).
43. J. van de Lagemaat, D. Vanmaekelbergh, and J. J. Kelly, "Field-dependent charge carrier dynamics in GaN: excitonic effects," Appl. Phys. Lett. **85**, 958–960 (2004).